Mechanical and optical nanodevices in single-crystal quartz

Young-Ik Sohn, Rachel Miller, Vivek Venkataraman, and Marko Lončar

Citation: Appl. Phys. Lett. **111**, 263103 (2017);
View online: https://doi.org/10.1063/1.5008759
View Table of Contents: http://aip.scitation.org/toc/apl/111/26
Published by the American Institute of Physics

Mechanical and optical nanodevices in single-crystal quartz

Young-Ik Sohn,[1,a)] Rachel Miller,[1,2] Vivek Venkataraman,[1,3] and Marko Lončar[1]
[1]John A. Paulson School of Engineering and Applied Sciences, Harvard University, 29 Oxford Street, Cambridge, Massachusetts 02138, USA
[2]Department of NanoEngineering, University of California San Diego, La Jolla, California 92093, USA
[3]Department of Electrical Engineering, Indian Institute of Technology Delhi, New Delhi, India

(Received 9 October 2017; accepted 14 December 2017; published online 27 December 2017)

Single-crystal α-quartz, one of the most widely used piezoelectric materials, has enabled a wide range of timing applications. Owing to the fact that an integrated thin-film based quartz platform is not available, most of these applications rely on macroscopic, bulk crystal-based devices. Here, we show that the Faraday cage angled-etching technique can be used to realize nanoscale electromechanical and photonic devices in quartz. Using this approach, we demonstrate quartz nanomechanical cantilevers and ring resonators featuring Qs of 4900 and 8900, respectively. *Published by AIP Publishing.* https://doi.org/10.1063/1.5008759

Silicon dioxide (SiO_2), the most abundant mineral found in the earth's crust, has eleven crystalline polymorphs determined by the temperature and pressure of the environment during the time of crystallization. Two of these are referred to as quartz: α-quartz is stable below 573 °C and β-quartz is stable above this temperature. α-quartz does not have a centro-symmetric crystal structure,[1] which is the cause for its piezoelectric response that allows the coupling between electrical and mechanical degrees of freedom. Furthermore, owing to quartz's crystalline anisotropy, dozens of substrates in different cut planes can be realized. The plane of crystal cut determines the characteristics of quartz devices such as resonant frequency, temperature coefficient of frequency (TCF), stability, and many others.[2] For example, AT-cut quartz is of great interest for temperature-insensitive crystal oscillators, whereas Z-cut is a common choice for tuning forks in watches.[3] In the rest of this manuscript, we refer to α-quartz as "quartz," for simplicity.

Quartz is also a promising material for nanophotonic devices and systems. High purity silica glass, with its low loss and large transparency window, was the key element that enabled low-loss optical fiber technology and long-distance communications. Silica is also a popular material for nonlinear optics and nanophotonics.[4] Compared to amorphous silica, quartz has lower optical loss while having the advantage of fast tuning of refractive index via electro-optic effect.[5] This combination makes quartz a unique material for achieving an ultra-high optical quality factor and electrical tuning simultaneously for whispering gallery mode resonators.[6]

In order to take full advantages of quartz's remarkable material properties, it is important to enhance interaction between the material and the electric field (optical or DC), which can be accomplished using nanoscale devices. However, high quality thin quartz films on foreign substrates are not available.[7] Yet, this is important for both electromechanical devices, where a sacrificial substrate is needed, and optical (and optomechanical) devices, where the substrate plays the role of cladding. Notable developments of the thin film platform for quartz include epitaxial growth on silicon substrates[8] and wafer-to-wafer bonding of quartz and silicon.[9] However, both methods have their own challenges. In order to realize devices in quartz, traditionally, wet etching of quartz has been most widely used. However, its anisotropic nature makes miniaturization difficult and causes unwanted features.[10] Deep reactive-ion etching has been proposed as an alternative to etch along any crystal axis.[11] In this work, we demonstrate functional nanomechanical and photonic devices in bulk quartz crystals using the modified dry etching approach.

Our approach [Fig. 1(a)] is based on Faraday cage angled-etching[12] that we have used to realize devices in bulk single-crystal diamond.[13] For the angled-etching step [Fig. 1(a)(vi)], we placed an aluminum Faraday cage of a conical shape about 1-in. high inside the reactive-ion etching chamber with the sample inside. This allows us to etch the sample at an oblique angle because the cage can make the trajectory of incoming ions approximately perpendicular to the lateral surface of it, by changing the boundary condition of the electric field potential.[12] Starting from the bulk quartz samples (purchased from SPI Supplies, double side polished), etch mask is defined using two different methods. Specifically, the standard bi-layer lift-off process was used to define an etch mask for cantilevers, while the mask pattern was transferred from e-beam resist to the sputtered metal film for microring resonators. The latter results in smoother mask and minimizes scattering loss of optical resonators, which is difficult to achieve with the lift-off process. Etch parameters and the type of reactive-ion etching tool used are described in our previous work.[12] This approach can make fairly complex structures in quartz, including double-ended tuning fork [Figs. 1(b) and 1(c)] and microring resonators (Fig. 4).

To show that our approach is applicable to different crystal cuts, cantilevers with similar dimensions have been fabricated by the same procedure in both AT-cut and Z-cut single-quartz crystals [Fig. 1(c)]. In both cases, fabricated cantilevers had widths in the 250 nm–350 nm range and lengths in the 5 μm–45 μm range. The thickness to width ratio was approximately 3.5 for all devices we used in the study, which can be tuned by adjusting the vertical position

a)Electronic mail: sohn@seas.harvard.edu.

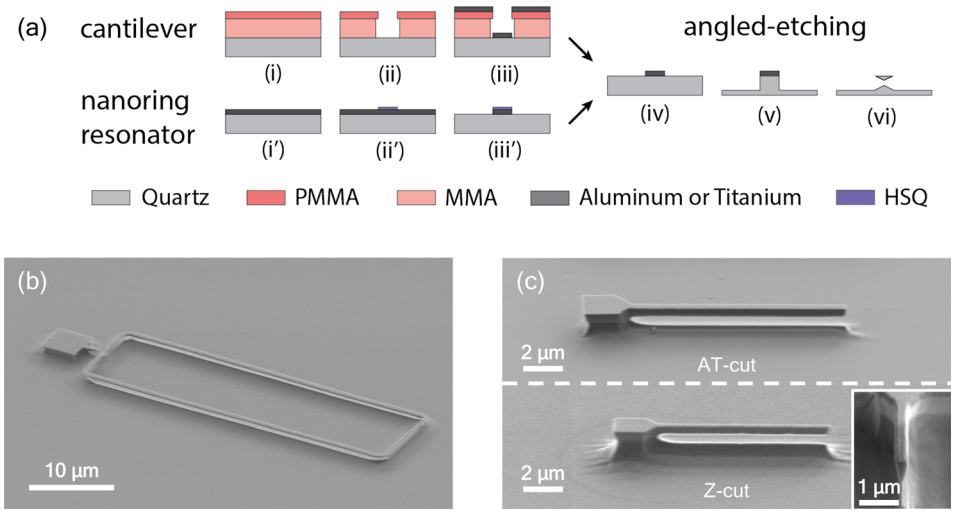

FIG. 1. (a) Schematic illustration shows the fabrication process of the cantilever and microring resonators. To define cantilevers, the aluminum mask is deposited using the standard bi-layer lift-off process. For ring resonators, the titanium film was first sputtered on quartz, and then, e-beam lithography and metal etching were used to define the mask. Next, the angled-etching step is performed to fabricate (b) a double-ended tuning fork and (c) cantilevers, made of quartz with two different crystal cuts. The inset shows the cross-section of the cantilever made of Z-cut quartz seen at a tilt angle of 52. The cantilever was cut with a focused ion beam to reveal the shape of the triangular cross-section.

of the sample during angled-etching. We expect that our approach can be applied to all existing crystal cuts of quartz, as discussed previously in the literature.[2,11]

To control the uniformity of the cantilever width better, we fabricated another chip with twenty eight cantilevers in the Z-cut quartz substrate, having the same cross-section with the width of 280 nm and lengths in the range of 9–24 μm. The neutral axis of all cantilevers is along the $\langle 1\,1\text{–}2\,0 \rangle$ direction of the quartz crystal. We measured thermal fluctuations of cantilevers in their fundamental flexural mode by optical interferometric displacement detection.[14] Fitting the Lorentzian function to thermal fluctuations, we can estimate the mechanical quality factor of the resonances. Figure 2(a) shows thermal fluctuations of cantilevers with different lengths in normalized power spectral density, with shifted resonance frequencies. We note the trend of increasing mechanical quality factor with the increasing length. To understand this trend and the mechanism that limits quality factors, we have taken statistics of all cantilevers with different lengths, where we have at least three cantilevers for each length. We plotted the average mechanical quality factors as a function of lengths in Fig. 2(b), with vertical bars indicating the standard deviation of measured devices. Using the theory of mechanical loss of cantilevers, we can fit our data to the following model:[15]

$$Q_{\text{total}}^{-1} = Q_{\text{clamping}}^{-1} + Q_{\text{other}}^{-1} = KL^{-1} + Q_{\text{other}}^{-1}, \tag{1}$$

where Q_{total} is the total mechanical quality factor we measure. The first and the second term on the right hand side account for the clamping loss and the rest of the loss mechanism, respectively. L is the length of a cantilever, and K is a fitting parameter that is a constant. Clamping loss is well studied theoretically and experimentally. When the width and the thickness of a cantilever are fixed, it is known that the loss rate is proportional to L^{-x} where the value of exponent x depends on the physical shape of clamping.[15] By inspecting the shape of the clamp shown in Fig. 1(c), we assume that the clamp behaves similar to that of out-of-plane motion with a large undercut,[15] and therefore, the exponent

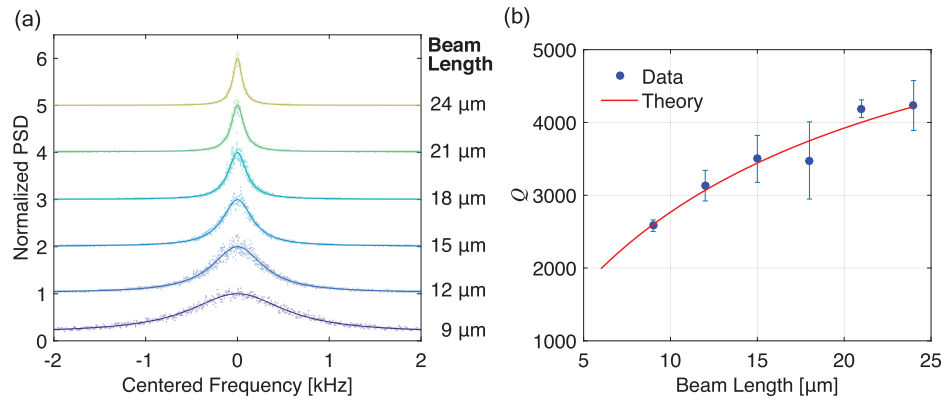

FIG. 2. (a) Normalized power spectral density (PSD) of thermal fluctuations of cantilevers at different lengths. Longer cantilevers give better mechanical quality factors because of the smaller clamping loss. Dots are raw data, and the solid lines are from the fit of Lorentzian functions. (b) A few dozen cantilevers are measured, and their statistics of mechanical quality factors are fit to the model described in the main text. Vertical error bars represent standard deviations of measured cantilevers with the same length. All the cantilevers are made of the same Z-cut quartz substrate.

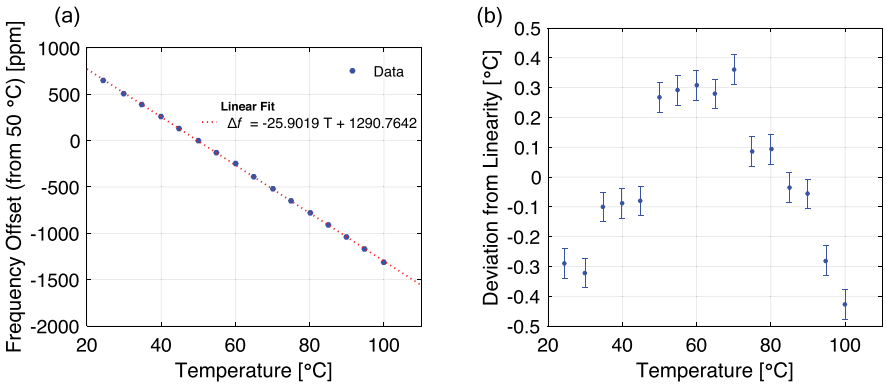

FIG. 3. (a) Resonance frequency of the 12 μm long cantilever as a function of temperature. The linear fit gives the value of the first order TCF. Standard errors of frequency and temperature for each measurement are smaller than the size of dots, and hence, they are not shown. (b) Deviation from the linearity in (a) is plotted to show the expected accuracy of temperature reading when the device is used as a thermometer. Vertical bars represent reading errors from digital readout of the temperature sensor. The cantilever was made of a Z-cut quartz substrate.

in Eq. (1) is assumed to be –1. The loss mechanism other than clamping loss is assumed to be independent of beam length. By fitting Eq. (1) to the data, we get an estimation of $Q_{\text{other}} = 6750 \pm 1950$ (uncertainty is for 95% confidence interval), and this length-independent loss is typically caused by the surface loss.[15] Therefore, to increase the mechanical quality factor, surface loss needs to be mitigated by, for example, surface treatment or device geometry with a low surface to volume ratio.

We further measured the temperature dependence of the resonance frequency of the 12 μm long cantilever. Conventionally, quartz tuning forks can be used to make millimeter scale thermometers by using their thermal expansion and the temperature dependence of the stiffness tensor. TCF is typically expanded in polynomial series up to the third order[16]

$$f(T) = f(T_0)(1 + \alpha(T - T_0) + \beta(T - T_0)^2 + \gamma(T - T_0)^3), \tag{2}$$

where f is the resonance frequency and T_0 is the operating temperature. α, β, and γ are temperature coefficients of the first, second, and third order, respectively. With a careful choice of crystal cut and the direction of neutral axes of the tuning fork's tines, it is possible to make a temperature sensor of a good linear response (large α and small β and γ) over a wide frequency range.[17]

Noting a flexural mode of a cantilever that is fundamentally similar to that of tuning forks, we measured the temperature sensitivity of its resonance frequency. By increasing the temperature with steps of 5 °C from 25 °C to 100 °C using a resistive heater and a closed-loop temperature controller (Thorlabs HT10K and TC200), we measured the response shown in Fig. 3(a). Fitting a linear curve gives the first order TCF of –25.9 ppm/°C. From the data, we calculated the deviation from the linearity as the difference between the fit model and measured temperatures. Figure 3(b) shows that the deviations fall within ±0.5 °C.

Nanophotonic devices can also be made using angled-etching, where air surrounding the structure is used as a cladding [Fig. 4(a)]. Slight widening of the width in the straight part of the resonator provides structural support.[18] A width of 1.5 μm was used to target the operating wavelength range in telecom. Enlarged SEM images in Fig. 4(a) reveal the visible surface roughness. We measured its optical quality factor using a tapered fiber setup whose image is shown in Fig. 4(b).[18] Figure 4(c) shows the transmission of the fiber that has resonances as a series of dips which originate from the evanescent coupling between the resonator and the fiber. We extract quality factors of each resonance from their widths by fitting Lorentzian functions. All the resonances have loaded quality factors on the order of thousands, and the highest of them is $Q_{\text{total}} = 8900$ as shown in the inset of Fig. 4(c). From the fitting, we estimate the intrinsic quality factor of approximately $Q_{\text{intrinsic}} = 13\,000$.[19] The quality factor at this level is lower than those of similar devices made on diamond.[18,20,21] Judging from images in Fig. 4(a), we believe that the limiting mechanism of optical quality factors is the surface roughness. By improving the fabrication process (i.e., using a better etching mask material or dry etch recipe), we expect to increase optical quality factors.

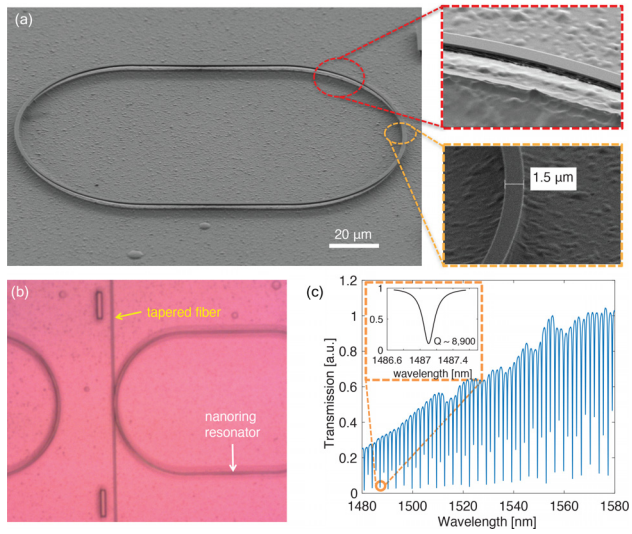

FIG. 4. (a) SEM image of microring resonators whose operation wavelength range is telecom. (b) Microscopy image of the fiber coupling setup where the light couples from the single-mode tapered fiber to a microring resonator. (c) Transmission measurement taken from the setup pictured in (b). Dips correspond to resonance conditions, and quality factors can be extracted from the widths of each dip. Loaded quality factors are on the order of thousands, and the largest ($Q \sim 8900$) is shown in the inset.

In summary, we have applied the Faraday cage angled-etching technique to single-crystal quartz and fabricated suspended structures with substrates of different crystal cuts. First, we made cantilevers with a nanoscale width and a high aspect ratio. By analyzing the trend of the mechanical quality factor as a function of cantilevers' lengths, we estimate the contribution of the surface loss to the quality factor to be on the order of thousands. With one of these cantilevers, we further measured the linear dependence of the resonance frequency on temperature. Finally, optical microring resonators for telecom wavelength were fabricated and their quality factors were measured. From the fitting, we estimated the intrinsic quality factor about ten thousands, where we presume that the loss is limited by a rough surface.

In the future, to make devices of practical use, we propose several approaches in the following. First, the current etch recipe described in Ref. 12 can be improved to fabricate better devices. Surface quality of the fabrication in this work seems to be limiting the quality factors for both mechanical and optical devices. Therefore, a better fabrication process can potentially lead to higher quality factors for both types. Second, well-studied characteristics of different quartz crystal cuts can be exploited in combination with our approach to fabricate various functional devices at the nanoscale, in a similar fashion to traditional engineering. For example, it is possible to engineer TCF by choosing different crystal cuts. Third, piezoelectric and electro-optic devices can be made by placing electrodes nearby. We have previously demonstrated the electrode patterning near diamond nanodevices are made from angled-etching.[22,23] Combining those electrodes with mechanical and optical elements in this work, we expect to fabricate more advanced piezoelectric or electro-optic nanodevices.

Y.-I. Sohn would like to thank P. Latawiec for helpful discussions on optimizing the etch recipe. This work was supported by the STC Center for Integrated Quantum Materials, NSF Grant No. DMR-1231319 and NSF GOALI Grant No. 1507508. Samples were fabricated at the Center for Nanoscale Systems (CNS), a member of the National Nanotechnology Infrastructure Network (NNIN), which was supported by the National Science Foundation under NSF Award No. ECS-0335765. CNS is part of Harvard University. R. Miller acknowledges the support provided by the National Nanoscale Infrastructure Network REU Program and the National Science Foundation under Grant No. ECCS-0335765.

[1]R. Newnham, *Properties of Materials: Anisotropy, Symmetry, Structure* (OUP Oxford, 2004).
[2]E. A. Vittoz, *Low-Power Crystal and MEMS Oscillators* (Springer, 2010).
[3]J. M. Friedt and É. Carry, "Introduction to the quartz tuning fork," Am. J. Phys. **75**, 415–422 (2007).
[4]G. P. Agrawal, *Nonlinear Fiber Optics* (Academic Press, 2013).
[5]G. Li, K. A. Winick, A. A. Said, M. Dugan, and P. Bado, "Waveguide electro-optic modulator in fused silica fabricated by femtosecond laser direct writing and thermal poling," Opt. Lett. **31**, 739 (2006).
[6]V. S. Ilchenko, A. A. Savchenkov, J. Byrd, I. Solomatine, A. B. Matsko, D. Seidel, and L. Maleki, "Crystal quartz optical whispering-gallery resonators," Opt. Lett. **33**, 1569–1571 (2008).
[7]C. J. Brinker and P. G. Clem, "Quartz on silicon," Science **340**, 818–819 (2013).
[8]A. Carretero-Genevrier, M. Gich, L. Picas, and J. Gazquez, "Soft-chemistry–based routes to epitaxial α-quartz thin films with tunable textures," Science **340**, 827–831 (2013).
[9]B. Imbert, A. Reinhardt, T. Ricart, C. Billard, E. Defaý, H. Virieux, T. Jouanneau, F. Pierre, V. Delaye, and P. Gergaud, "Thin film quartz layer reported on silicon," in *Frequency Control and the European Frequency and Time Forum (FCS), 2011 Joint Conference of the IEEE International* (IEEE, 2011), pp. 1–4.
[10]A. Kamijo, S. Monoe, N. Murayama, T. Saito, and N. Kimura, "Wafer-level quartz dry etching technology," in *2014 IEEE International Frequency Control Symposium (FCS)* (IEEE), pp. 1–4.
[11]P. Chapellier, P. Lavenus, B. Bourgeteau-Verlhac, C. Gageant, O. L. Traon, and B. Dulmet, "Aspect ratio dependent etching in advanced deep reactive ion etching of quartz," in *2017 Symposium on Design, Test, Integration and Packaging of MEMS/MOEMS (DTIP)* (IEEE), pp. 1–6.
[12]P. Latawiec, M. J. Burek, Y.-I. Sohn, and M. Loncar, "Faraday cage angled-etching of nanostructures in bulk dielectrics," J. Vac. Sci. Technol. B **34**, 041801 (2016).
[13]M. J. Burek, N. P. de Leon, B. J. Shields, B. J. M. Hausmann, Y. Chu, Q. Quan, A. S. Zibrov, H. Park, M. D. Lukin, and M. Loncar, "Free-standing mechanical and photonic nanostructures in single-crystal diamond," Nano Lett. **12**, 6084–6089 (2012).
[14]D. Karabacak, T. Kouh, and K. L. Ekinci, "Analysis of optical interferometric displacement detection in nanoelectromechanical systems," J. Appl. Phys. **98**, 124309 (2005).
[15]M. Imboden and P. Mohanty, "Dissipation in nanoelectromechanical systems," Phys. Rep. **534**, 89–146 (2014).
[16]X. Jun, B. You, L. Xin, and C. Juan, "Theoretical model and optimization of a novel temperature sensor based on quartz tuning fork resonators," Phys. Scripta **129**, 316–320 (2007).
[17]T. Ueda, F. Kohsaka, T. Iino, and D. Yamazaki, "Temperature sensor using quartz tuning fork resonator," in *40th Annual Symposium on Frequency Control. 1986* (IEEE, 1986) pp. 224–229.
[18]M. J. Burek, Y. Chu, M. S. Z. Liddy, P. Patel, J. Rochman, S. Meesala, W. Hong, Q. Quan, M. D. Lukin, and M. Loncar, "High quality-factor optical nanocavities in bulk single-crystal diamond," Nat. Commun. **5**, 5718–5718 (2014).
[19]S. M. Spillane, T. J. Kippenberg, O. J. Painter, and K. Vahala, "Ideality in a fiber-taper-coupled microresonator system for application to cavity quantum electrodynamics," Phys. Rev. Lett. **91**, 043902 (2003).
[20]H. A. Atikian, P. Latawiec, M. J. Burek, Y.-I. Sohn, S. Meesala, N. Gravel, A. B. Kouki, and M. Loncar, "Freestanding nanostructures via reactive ion beam angled etching," APL Photonics **2**, 051301 (2017).
[21]P. Latawiec, M. J. Burek, V. Venkataraman, and M. Loncar, "Waveguide-loaded silica fibers for coupling to high-index micro-resonators," Appl. Phys. Lett. **108**, 031103 (2016).
[22]Y.-I. Sohn, M. J. Burek, V. Kara, R. Kearns, and M. Loncar, "Dynamic actuation of single-crystal diamond nanobeams," Appl. Phys. Lett. **107**, 243106 (2015).
[23]Y.-I. Sohn, S. Meesala, B. Pingault, H. A. Atikian, J. Holzgrafe, M. Gündoğan, C. Stavrakas, M. J. Stanley, A. Sipahigil, J. Choi, M. Zhang, J. L. Pacheco, J. Abraham, E. Bielejec, M. D. Lukin, M. Atatüre, and M. Loncar, "Engineering a diamond spin-qubit with a nano-electro-mechanical system," preprint arXiv:1706.03881v1 (2017).